Analytical Methods

ROYAL SOCIETY OF CHEMISTRY

TECHNICAL NOTE

View Article Online
View Journal | View Issue

Cite this: *Anal. Methods*, 2025, **17**, 5973

3D-printed accessories for nano/microelectrodes†

Cody W. Leasor, Kelly L. Vernon, Yunong Wang, Reed E. Baker and Lane A. Baker *

Received 21st May 2025
Accepted 30th June 2025

DOI: 10.1039/d5ay00865d

rsc.li/methods

Rapid prototyping and 3D-printed devices have become important enabling technologies for measurement science. Work presented here aims to add to the 3D-printed toolset by demonstrating the economical production and application of printed centrifuge and electrode holders for micro and nanoelectrodes. These holders provide freedom of configuration and design and can also circumvent availability issues which may exist for commercial electrode holders. Here we demonstrate 3D-printed centrifuge holders which aid in filling small pipettes with fluid and 3D-printed electrode holders used both in electroanalytical probe characterization and in scanning ion conductance microscopy.

Introduction

Rapid prototyping by 3D printing has become an increasingly popular approach for tool development.[1,2] Applications in analytical chemistry include development of macroscale electrode holders,[3] electrochemical sensors,[4–10] colorimetric devices,[11–13] multi-modal microfluidic devices,[14–25] and customized mass spectrometry ionization chambers,[26] in addition to other areas of analytical chemistry such as chromatography, extraction and spectroscopy.[8] Micromanipulators and probe positioners for scanning probe microscopy (SPM) have also been explored.[27] For instance, components printed to mount stepper motors for use in construction of a simple and economical electrochemical-scanning probe microscope have been demonstrated.[28] Here we describe, cost-effective and reliable routes to micro and nanoelectrode holders that can be easily customized as needed.

Commercial microelectrode holders, often used for electrophysiology and scanning ion conductance microscopy (SICM),[29–31] can be purchased, but supply and configuration of holders are often limited. Commercial microelectrode holders are typically machined from polymeric materials (such as polycarbonate) in a traditional top-down machining approach. Variations in holder configuration can also complicate incorporation into hardware that mounts holders for applications (*e.g.* performing/setting up SPM experiments). With these aspects in mind, 3D printing is recognized as an approach to aid in fabrication of components to facilitate use of micro and nanoelectrodes.

Work described here adds to the rapid prototyping-based toolset for analytical chemistry through stereolithography (SLA) and masked-SLA (MSLA) 3D printing that aided in the development of single and theta barrel electrode holders with form factors inspired by previous commercial designs. The central body of single- and theta-barrel electrode holders are generated with two different 3D printing platforms (Phrozen Sonic Mini 8K and Formlabs Form2 3D printers) combined with simple hand tooling. Incorporation of ancillary off-the-shelf components are used to complete assemblies. Additionally, we detail "centrifuge holders", which are adapters for filling pipettes *via* centrifugation, a valuable tool especially for filling small single-barrel pipettes. A key advantage of 3D printing electrode holders is the ability to generate additional configurations tailored to suit applications. Examples of this are demonstrated with holder designs that add a port to the body of the holder for pressure connections[32,33] and that add additional connections for electrodes.

Experimental

General 3D printing parameters

Printed pieces were designed in SOLIDWORKS, and either CHITUBOX or PREFORM slicer software were used to convert SOLIDWORKS' .STL files to printable files (part orientations and parameters for prints are given in Fig. S1†). A Phrozen sonic Mini 8K (MSLA) 3D printer with Aqua Clear resin was used for translucent holder production, whereas a Formlabs Form2 (SLA) 3D printer with Rigid 10K resin was used for more steadfast holder production. Translucent centrifuge holders were printed in one run, while electrode holders (whether they be the translucent or rigid holders) were printed in separate runs. Typical prints took approximately 5–6 hours for the centrifuge holders (using a recommended slice resolution setting of 50 μm), 36 hours for the translucent electrode holders (10 μm slice resolution) and approximately 5–6 hours for rigid electrode holders (also utilizing the recommended 50 μm slice resolution). When finished, prints were vented under ambient

Department of Chemistry, Texas A&M University, College Station, TX, 77845, USA. E-mail: lane.baker@tamu.edu

† Electronic supplementary information (ESI) available: Raw data and CAD files. See DOI: https://doi.org/10.1039/d5ay00865d

conditions for a minimum of 30 minutes, then removed from the printer platform. A 30-second wash of each piece was performed using 200 proof ethanol for all Phrozen prints and two 10-minute washes, one with water and another with isopropyl alcohol, for all Formlabs prints.

An Elegoo Mercury Plus post cure device was used to finalize the curing stage of the Phrozen prints. Resin manufacturers suggest 40 miuntes to 1-hour of UV exposure (at room temperature for Aqua Clear prints and at 70 °C for Rigid 10K prints) to fully cure, however, the long exposure to the UV light caused the clear-colorless prints to discolor, resulting in a yellow tint (Fig. S2a†). As a result, the post curing UV exposure was limited to 5 minutes, to prevent discoloration (Fig. S2b†), for the Aqua Clear prints. An attempt to find the minimal time needed to finish the post curing process before discoloration was performed. Longer cure times (*e.g.* 40- to 60 minutes, as suggested by manufacturer) were not employed, as these times led to discoloration. Of note, manufacturer curing times are approximate, and do not consider the intensity or configuration of specific UV-curing stations. In the procedures we employed, cure times of 5–10 minutes were found to provide suitable cosmetic properties and mechanical strength for pieces generated.

After curing, support structures were removed and any cosmetic issues were corrected (*e.g.*, smoothing and/or flattening of surfaces by sanding/buffing, and occasionally re-threading *via* taps and dies). After corrections, if needed, a thin layer of resin was painted onto parts and cured for 5 minutes, to make the print more transparent (Fig. S2b†).

Centrifuge holder printing

Difficulties in wetting and surface tension can make filling small pipettes problematic. Centrifuging small pipettes is a useful method to fill tips but requires a "centrifuge holder". Centrifuge holders for this purpose were 3D-printed to increase the success of filling nanopipettes without damaging the pipette tip. Individual and assembled holders for pipette filling are shown in Fig. 1a. Centrifuge holders are made up of a body that fits snuggly in a 2 mL centrifuge tube, suitable for use in mini centrifuges. The top of the central body has a recessed lip to provide grip for separating the central body and centrifuge tube if the body becomes seated too firmly after centrifugation. The other end of the central body is threaded to mate a threaded "end cap". A through-hole, dimensioned to pass a capillary of a given diameter, runs the entire length of both the central body and end cap. A gasket, mounted between the central body and end cap is compressed when the two pieces are tightened, which squeezes the capillary gently, but sufficiently to survive centrifugation. The designs shown in Fig. S3,† have a through-hole inner diameter of 1.5 mm, which can accommodate single (left drawing views in Fig. S3†) or theta barrel pipettes (middle drawing views in Fig. S3†) typically used for SICM. Gaskets were made from drilling a through-hole in a flat sheet of silicone rubber (3–4 mm thick), dimensioned to match the outer diameter of capillaries (1.0 mm for single barrel capillaries; 1.2 mm for theta barrel capillaries) and were then punched out of the rubber sheet with an outer diameter of 4–4.5 mm (Fig. S4a†).

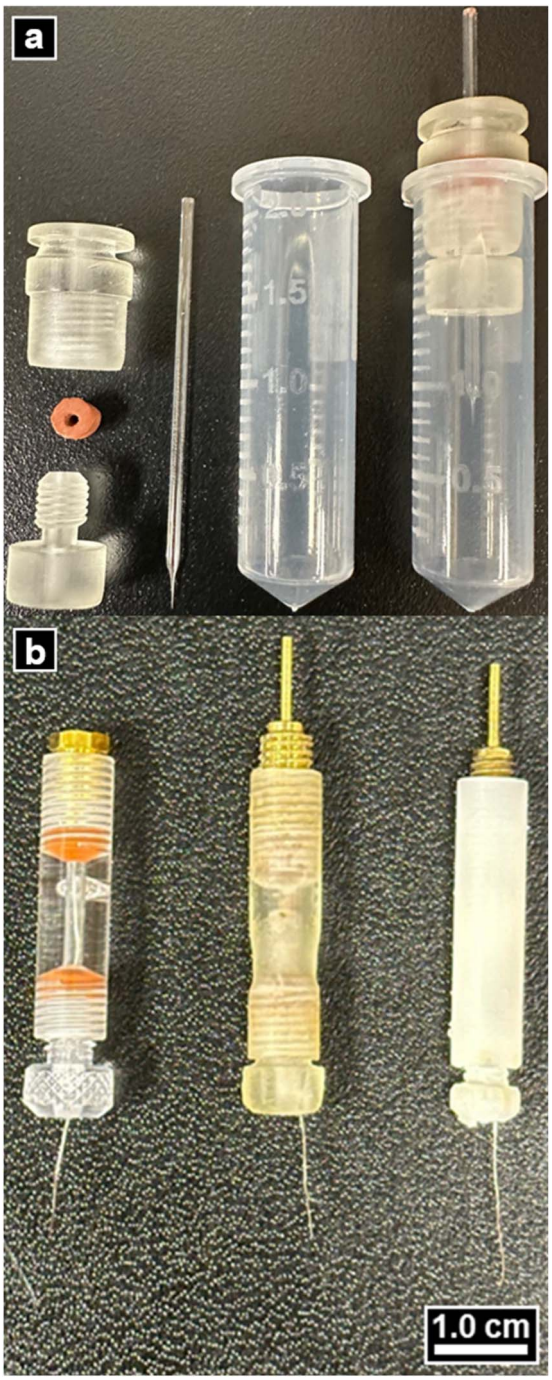

Fig. 1 Nanopipette centrifuge and electrode holders. (a) Photograph of (left to right) a dissembled centrifuge holder, a nanopipette, a 2-mL centrifuge tube and the probe filling assembly. (b) Photograph of the three single barrel electrode holders used in this study. Left to right is a transparent commercial (acrylic), fabricated translucent and fabricated rigid electrode holders, assembled with a Ag/AgCl wire.

Electrode holder printing

Electrode holders (Fig. 1b) were printed in a manner similar to that described for centrifuge holders (see Fig. S3† for

dimensions). Electrical connectors were incorporated with PCB solder mount micro-jacks (Mouser electronics, Mansfield, TX) that were soldered to machined M5 screws that had a through-hole of 3 mm inner diameter (left and middle of Fig. S4b and c†). This was done for both double barrel electrode holders. For single barrel holders, electrical connection was achieved by machining an M5 screw with an extending pin (without the need to solder a micro-jack into a bolt, right of Fig. S4b and d†). These connections would then mate with their respective, threaded electrode holder ports, shown in Fig. 2 in exploded and assembled views (left and right SOLIDWORKS drawings, respectively).

Coated silver wire (diameter of 0.005 inches (A-M systems, Sequim, WA)) was used as an electrode inside the pipette. To aid in electrical connection, the polymer coating on each end of the wire was mechanically sheared to expose 1–2 cm of the silver wire, on both ends. One of the exposed ends was soaked in 0.1 M $FeCl_3$ and 0.1 M HCl for 6–8 hours and rinsed thoroughly with purified water (18.2 M cm). The Ag/AgCl wire was fed through the electrode holder and connections made with cold contact (mechanically forced electrical connection) between the micro-jacks and the wire that is compressed and sandwiched between the brass bolt and the rubber gasket as shown in the images in Fig. 2. The physical mechanism for this type of cold contact electrical connection is the bases for all electrode holders, commercial and fabricated like those shown in Fig. 1b.

Nanopipette fabrication

Single barrel pipettes with *ca.* 80 nm inner diameter, were fabricated from quartz glass capillaries with an outer diameter of 1.0 mm, inner diameter of 0.7 mm and length of 7.5 cm (Sutter Instruments, Novato, CA). The single barrel capillaries were pulled with a P-2000 CO_2 laser puller (Sutter Instruments, Novato, CA) and the following settings: HEAT = 610, FIL = 3, VEL = 40, DEL = 180, PULL = 155. Theta barrel pipettes with *ca.* 80 nm inner diameter (for each barrel), were fabricated from quartz theta capillaries with an outer diameter of 1.2 mm, inner diameter of 0.9 mm and length of 7.5 cm (Sutter Instruments, Novato, CA). The theta barrel capillaries were pulled with the following settings: HEAT = 713, FIL = 3, VEL = 35, DEL = 200, PULL = 150. All capillaries were mounted into the P-2000 puller's padded pully system with a hex key tighten to 25 cN m with the use of a Bestool–Kanon torque screwdriver.[34]

Filling nanopipettes

Purified water (18.2 MΩ cm, Barnstead GenPure Pro (Thermo Scientific, Houston, TX)) was used to make 0.1 M KCl (Sigma-Aldrich, St. Louis, MO) for all electrochemical bath and probe filling solutions. A microfil flexible needle (World Precision Instruments, Sarasota, FL) was attached to a Nylon 0.20 μm syringe filter (Wheaton Science Products, Millville, NJ) that junctions the microfil to a 1-mL syringe that contained 1 mL of pre-drawn 0.1 M KCl. Solution was dispensed into the pipette barrel, up to the initial tapering of the tip. This pre-fill volume ranged from 7 to 10 μL (half to three-quarters of the length of the pipette). The partially filled pipette was then placed in a centrifuge holder assembly (Fig. 1) housed with a 2-mL centrifuge tube (Alkali Scientific, Fort Lauderdale, FL).

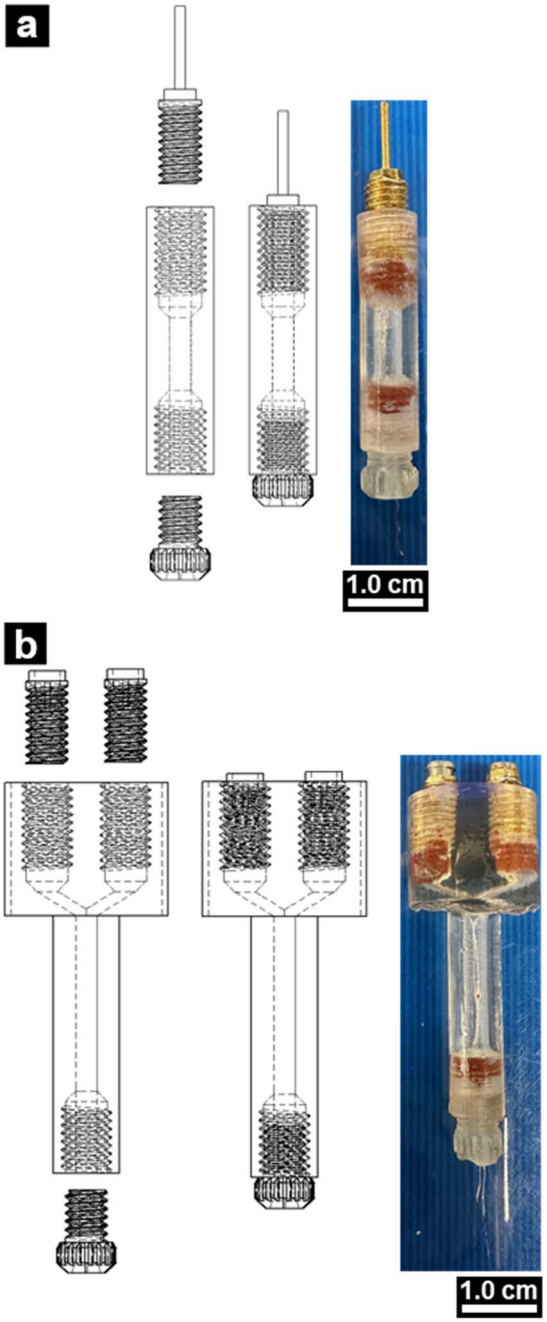

Fig. 2 Nanopipette microelectrode holders. (a and b) SOLIDWORKS drawings of an exploded view (left), assembled view (middle) and an image (right) of the fabricated single (top) and theta (bottom) electrode holders, respectively.

The assembly was then gently tapped on the side of the pipette barrel to mechanically dislodge any gas bubbles. A thin piece of single-sided Scotch tape was placed tightly around the back of each pipette, to provide additional assurance pipettes would not slide out of centrifuge holders when centrifuging. A heuristic approach was performed by altering centrifugation time and speed such that minimal pipette breakage was

observed while also giving reasonable responses to electrochemical measurements outlined in the following sub-section. These parameters are dependent on pipette geometry and solution viscosity and may need to be modified as needed. For pipettes employed here, an Eppendorf Mini-Spin centrifuge (Hamburg, Germany, motor radius of 6 cm) was employed to spin single barrel pipettes for 5 minutes at 8.6 thousand rotations per minute (krpm), or theta barrel pipettes for 7 minutes at 8.1 krpm (duration and spin rate vary based on dimensions of the pipette to be filled.)

Electrochemical measurements

Linear sweep voltammetry was used to obtain current–voltage responses (*I–V* curves) of the filled pipettes, using fabricated electrode holders. Electrodes (Ag/AgCl) were back inserted into the pipettes. A 6487 picoammeter/voltage source (Keithley Instruments, Solon, OH) was used to obtain *I–V* curves, where the source terminal was connected to the pipette electrode. The pipette was then immersed into a 0.1 M KCl bath that contained a second Ag/AgCl was connected to the ground terminal. Measurements were recorded in triplicate from −1 V to +1 V, at a scan rate of 0.1 V s^{-1} in increments of 0.1 V, after holding the potential at the initial value (−1 V) for a 2 second quiet time. Conductivities of the bath and filling solution were measured with a PC 700 conductivity meter (Oakton, Vernon Hills, IL).

Scanning ion conductance microscopy measurements

A home-built scanning ion conductance microscope, detailed in previous publications,[29–31] was used to collect topography maps of a polydimethylsiloxane (PDMS, Sylgard 184 Silicone Elastomer kit, Dow, Midland, MI) sample bathed in 0.1 M KCl electrolyte. The PDMS mixture was made by weighing 10-parts reagent A and 1-part reagent B from the elastomer kit, prior to thoroughly mixing the two reagents and then using a vacuum until all bubbles were removed. The elastomer standard replica (PDMS sample) was developed from a grating standard (Fig. 4),[35] where 1–2 mL of uncured PDMS was drop cast onto the original standard before spinning coating the uncured PDMS. Spin coating was done with a Polos spin coater (SPS Polos) at an initial spin acceleration of 100 rpm s^{-1} and held at 300 rpm for 20 s before ramping again at 500 rpm s^{-1} to a final 1500 rpm, which was held for 60 s, prior to decelerating to 0 rpm at a rate of 500 rpm s^{-1}.

The sample was then cured slowly overnight on top of a pre-heated oven at 120 °C. The PDMS mold was gently removed and placed into a 35 mm Petri dish where a small amount of uncured PDMS was painted on the edges of the sample to secure the mold to the Petri dish and left to cure at room temperature for 48 h. 0.2 V was applied to the pipette electrode with respect to a Ag/AgCl reference electrode that was also immersed into the electrolyte. Scanning was done at 2.0% threshold, 520 nm hop height, 30 μm × 30 μm scan area at 120 pixels × 120 pixels (250 nm per pixel resolution). Complete image collection for data shown required on the order of 50 minutes to complete. To minimize thermal drift, the probe was brought close to the sample surface and allowed to equilibrate thermally for 1–2 hours.[36] During this time, the inverted microscope light source or lamp was turned off to remove a source of thermal drift and the lamp remained off during all scans.

After equilibration, the probe was repositioned to an area of interest and a hopping mode raster scan was employed to collect topographical data. After the first scan, the probe assembly was removed and the pipette was placed in the commercial holder and mounted into the instrument prior to repeating the sample approach, thermal equilibrating wait time, probe repositioning and finally scanning over the same area. Topographical maps were cropped (30 μm × 22.5 μm and 120 pixels × 90 pixels) to focus on the same number of the PDMS sample's features, limited by one image only showing five completely imaged features, instead of the intended nine. Additionally, these images were levelled by mean plane subtraction and the resulting *Z*-height values were adjusted *via* shifting minimum data value to zero. After processing images in the same manner, the resulting Z-coloring scale for each image was adjusted from 0 to 380 nm. Raw data prior to processing is shown in Fig. S6.†

Potentiometric-scanning ion conductance microscopy (P-SICM), detailed in previous publications,[31,37,38] was performed on a polyimide membrane that was track-etched to have pores with nominal diameters of 2.5 μm. The membrane was encased in a tape mask that exposed a 1-mm-diameter circle from the sample center. The masked membrane was assembled in a perfusion cell[29] with a 0.1 M KCl bath on both faces of the membrane. A Ag/AgCl working electrode was placed in the bottom chamber and a Ag/AgCl reference electrode and Pt counter electrode were placed in the upper chamber. A potential of 0.2 V was applied to the pipette electrode with scanning parameters of 2.0% threshold, 2 μm hop height. A 200 mV_{PP} potential applied to the working electrode at a frequency of 5 Hz was used to generate potential gradients. SICM and P-SICM images were processed with Gwyddion and/or with a Python script.

Optical and scanning electron microscopy measurements

An ECHO rebel microscope (Discover Echo Inc., San Diego, CA) with 20× objective was used for obtaining images of pipettes during filling process. A Field Emission-Scanning Electron Microscoy (FE-SEM (JSM7500)) was used for obtaining end-on and side view micrographs of 11 nm Au/Pd (1 : 1) sputter coated pipettes. A JOEL Neoscope III benchtop SEM was used for obtaining images of the AFM standard sample. ImageJ FIJI was utilized for making calibrated measurements of SEM data and line profiles.

Results and discussion

Electrode connection for probe size estimation and validation

The pipette was pre-filled with 0.1 M KCl, then placed in the probe filling assembly (Fig. 1) and gently tapped to move the liquid down most of the tip taper. The assembly was then centrifuged to completely fill pipettes with electrolyte.

The current–voltage (*I–V*) response of pipettes was measured *via* linear sweep voltammetry, with each pipette (or barrel) measured in triplicate. *I–V* Curves recorded were plotted as a function of potential with standard error represented as the error bars for each point in Fig. 3a. The average and standard error for each point in the plot was calculated from the 9 barrels (3 single barrel and 3 theta barrel pipettes contributing 3 and 6 barrels, respectively) at a 90% confidence interval (CI).

This measurement is often used to estimate the probe tip size (r_{tip}) of single barrel ($r_{tip(single)}$) and theta barrel pipettes ($r_{tip(theta)}$) with back inserted electrodes. The inverse of the *I–V* curve's slope is the probe resistance (R_p), which can be easily calculated from the *I–V* curve response. We chose to measure current–voltage curves at concentrations relevant to the SICM experiments described here, which results in rectified current responses. When there is a rectified response, selection of data where minimal rectification occurs is optimal to estimate tip sizes based on the current–voltage response. Results from the linear equation and the observed rectified ion current as a function of absolute potential are shown in Fig. S5.† To estimate the pore size, values of ±0.1 V *vs.* Ag/AgCl were chosen where the ICRR effects are minimized. This potential window was used to calculate the inverse slope for each barrel's *I–V* curve. The equation used to estimate a single barrel's inner pipette tip size has been widely used in previous work[37,39] and is represented in eqn (1). To a first approximation, theta barrel pipettes tip dimensions can be estimated by halving this relationship (eqn (2)).[40]

$$r_{tip(single)} \approx \frac{\cot(\theta/2)}{\pi\kappa R_P} \quad (1)$$

$$r_{tip(theta)} \approx \frac{r_{i,single\text{-}barrel}}{2} \quad (2)$$

The solution conductivity (κ) and the pipette's half cone angle ($\theta/2$) are also required to estimate the inner pipette tip size. Side view SEM micrographs of sister pipettes (one of the two halves pulled from the original capillary) can be used to obtain the half cone angle.[41,42] In this respect, *I–V* curve data recorded from pipettes were collected (Fig. 3a), with their respective sister pipettes dedicated to SEM analysis (Fig. 3b and c left and right images).

The model to estimate the radius of the probe relies strongly on the conical taper at the end of the pipette tip. The majority of the resistance originates at the very tip of the pipette, and this region is where the half cone angle was measured (see Fig. S7†). The overall average half cone angle (both single and theta barrel probes) estimated was 6 ± 3°.

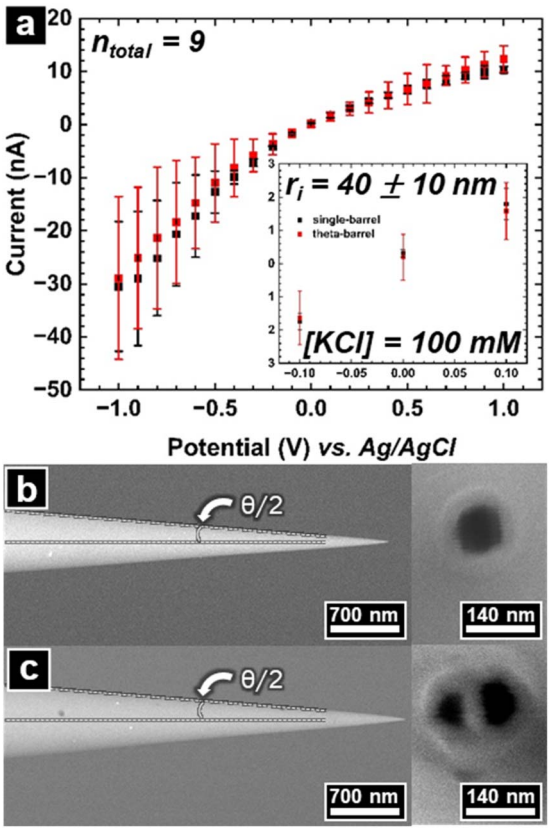

Fig. 3 Current–voltage response of (a) an averaged current–voltage response for 9 barrels (3 single barrels and 6 theta barrels or 3 theta probes) with standard error, error bars at 90% CI; inset is the middle three data points used for calculating the slope. (b and c) SEM micrographs of side view (left) and end-on view (right) of single and theta barrel pipettes, respectively.

Electrode holders' SICM application

Next, a PDMS casting of a grating standard (used as mold for PDMS curing) was fixed to a plastic Petri dish that contained 0.1 M KCl bath electrolyte. The SEM micrograph, shown in Fig. 4a, is a region of the grating standard mold prior to sample development (without sputter coating) with an array of square exclusions. These exclusions' lateral dimensions serve as a reference for SICM topographical mapping of the PDMS cast which were averaged and are reported with standard error (90% CI at $n = 5$) as 5.1 ± 0.3 μm × 5.0 ± 0.3 μm along the *x*- and *y*-direction, respectively (determined by calculating the full width at half maximum, FWHM, for each peak in the exclusions' line profiles and taking the difference of the mid-points along the *x*-axis at each of these values).

To validate the stability of single and theta barrel 3D-printed electrode holders for SICM measurements, pipette probes that were filled with 0.1 M KCl (same electrolyte and concentration as the sample's bath solution) and mounted in electrode holders were used to image the PDMS cast (Fig. 4b–d). Fig. 4b–d represents the topographical maps of the resulting square array regions, collected with commercial and fabricated (*i.e.*, Phrozen and Formlabs 3D-printed electrode holder), respectively.

The topography maps collected with the commercial (Fig. 4b) and Formlabs 3D-printed holders (Fig. 4d) appear more similar to one another than the topography map collected with the Phrozen 3D-printed holder (Fig. 4c) (of note, in Fig. 4c contrast is higher due to a sample defect seen in the middle of the image). The overall height of features relative to the average base height is consistent in all topography maps. Lastly, the

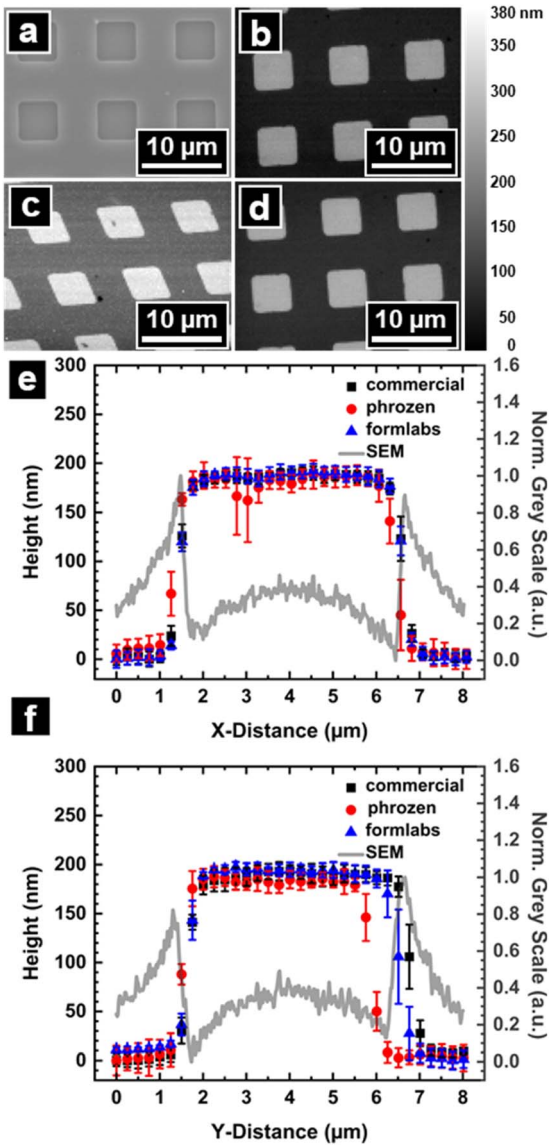

Fig. 4 SICM electrode holder evaluation. (a) SEM micrograph of a standard grating (without prior sputter coating the sample), used as a mold for a PDMS casted sample. (b–d) SICM topographical maps of the PDMS casted sample (cured onto and later removed from (a)), taken with a commercial, Phrozen 3D resin printed (Aqua Clear resin) and Formlabs 3D resin printed (Rigid 10K resin) single barrel electrode holder, respectively. (e and f) are the horizontal (*X*-distance) and vertical (*Y*-distance) line profiles of the sample's features displayed in (a–d), respectively, with corresponding error bars as standard errors at 90% CI and $n = 5$ (minimum number of completely imaged features amongst all topography maps).

topography map in Fig. 4c exhibits significant lateral distortion causing the features to appear as rhomboids rather than the square-like features observed in the reference SEM micrograph of Fig. 4a or the control data shown as the topographical map of Fig. 4b.

Quantitative analysis of the data in Fig. 4a–d was done by obtaining horizontal and vertical profiles of the features, that were completely imaged in topography maps. These profiles were then averaged and their respective standard errors (90% CI at $n = 5$) were estimated for each of the electrode holders. Data was plotted as a function of distance and was overlaid with the averaged profile data obtained in the SEM image for the horizontal (Fig. 4e) and vertical (Fig. 4f) profiles. Fig. 4e shows the horizontal profiles plotted as a function of *x*-distance, where the largest deviation was caused by a single square extrusion having a surface defect shown as a concavity within apical plane of the top-middle feature found in Fig. 4c. This surface defect did not have an influence on the vertical profiles as a function of *y*-distance shown in Fig. 4f. Instead, the only deviation appears to be the width of the features collected with the Phrozen 3D-printed electrode holders. Further analysis of this data was done by taking the average height of the features' apical section along each profile, which was used as the peak value when calculating the features' FWHM values that represent their length and width. The resulting lengths of the features found in Fig. 4e were 5.24 ± 0.04 μm, 5.13 ± 0.03 μm and 5.21 ± 0.02 μm for the commercial and fabricated Phrozen and Formlabs 3D-printed holders, respectively. Whereas the resulting widths of the features found in Fig. 4f were 5.17 ± 0.07 μm, 4.49 ± 0.04 μm and 4.92 ± 0.06 μm for the commercial and fabricated Phrozen and Formlabs 3D-printed holders, respectively.

Feature dimensions in the SEM data, was used as a reference for comparing how well each electrode holder performed while scanning to produce the data in Fig. 4. The resulting percent error for the measured extrusions' dimensions with a probe mounted in the commercial electrode holder was 3% error along both the horizontal and vertical, an acceptable amount of error for this measurement. However, the percent error for the measured features' dimensions with a probe mounted in the Phrozen fabricated electrode holder was 1% error along the horizontal and an alarming −10% error along the vertical, which is most likely due to the cause of the distortions observed in Fig. 4c. Comparisons of these results relative to data taken with the commercial holder showed a percent error at 2% along the horizontal and 13% along the vertical, further highlighting the distortions in Fig. 4c from the data in Fig. 4b. Whereas, the percent error for the Formlabs fabricated electrode holder, relative to SEM data, was 2% along the horizontal and 2% along the vertical, which suggests the electrode holder fabricated from the Formlabs printer relative to the Phrozen 3D printer appears to have nominally higher accuracy in feature sizes imaged, taking the commercial holder as ground-truth. Comparing the Formlabs electrode holder data relative to the commercial electrode holder data, the percent error was 1% along the horizontal and 5% along the vertical, which continues to highlight the fact that imaging done with these two types of electrode holders are very comparable and produce similar data.

The cause of distortion in Fig. 4c was assessed to lateral drift. This was observed *via* optical microscopy with images taken before and after the scan relative to a defined position (refer to Fig. S8†). The recording of these observations of drift were part of the imaging protocol before and after each scan taken for each one of the electrode holders. Phrozen electrode holder exhibited the greatest drift compared to the other two electrode holders used to collect topographic data. The reason for the

drift is assumed to be the only main difference between the electrode holders, which is the material that makes up their bodies. Commercial electrode holders are advertised as being composed from a variety of materials, including polycarbonate or acrylic materials (the material parameters that would most closely associate with thermal drift are thermal expansion coefficients). Formlabs provides a thermal expansion coefficient for the cured Rigid 10K resin of 41×10^{-6} °C^{-1} (within 0 to 150 °C). The Phrozen Aqua Clear resin does not have a published thermal expansion coefficient, but is advertised as being able to bend slightly, giving the impression that the thermal expansion coefficient is possibly higher than either of the other two materials. This would explain why the data obtained from the commercial and Formlabs 3D-printed electrode holders were comparable.

The 3D-printed holders were also employed in P-SICM, as shown in Fig. 5. Here a porous polyimide membrane separated the upper and lower chambers of a perfusion cell that are filled with the same electrolyte (0.1 M KCl). Topographical and local apparent conductance maps of micrometer-sized pores of the membrane were collected simultaneously. Fig. 5a shows the topographical map which clearly denotes that there are at least two complete pores visualized within this image. Fig. 5b presents the corresponding local apparent conductance map, with higher conductance values at or near the pores located in the topographical map, compared to values over the membrane.

Moreover, the electric field emanates beyond the physical dimension of the pore in the conductance map, which makes the pores appear larger than the size seen in Fig. 5a. This is observed as a broadened conductance spike over the pore which is caused by a small hop height relative to the physical radii of the pores.[38,43] To further correlate the position of pores in Fig. 5a with the conductance measured in Fig. 5b, an overlaid image is shown in Fig. 5c. The data shown in Fig. 5c displays color gradient array of pixels along the lateral points of the scan that are positioned along the *z*-direction coordinating with the heights displayed in Fig. 5a and given a color that coordinates with the data in Fig. 5b. This clearly shows that the highest regions of the measured conductance are that over/into the pore with heights closer to 0 μm and regions of lower conductance were measured over the membrane where pores are not present. The evidence obtained from Fig. 5 demonstrates 3D-printed electrode holders can be used to obtain more than just traditional SICM topographic data and presents an avenue for others to further customize electrode holders to experimental needs.

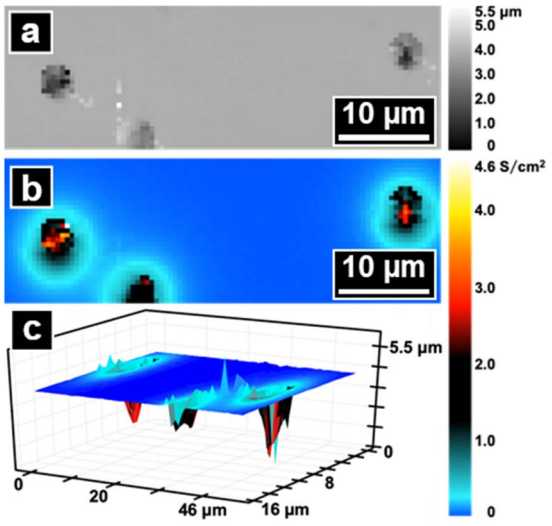

Fig. 5 P-SICM of a porous sample. (a and b) Correlating topographical and local apparent conductance maps of a couple of pores in a polyimide membrane. (c) The same data in (a and b) but displayed as a 3D image where the individual pixel color corresponds to measured local apparent conductance.

Conclusions

This work demonstrates that 3D-printed centrifuge holders and microelectrode holders can be easily manufactured in configurations suitable for electroanalytical applications. Electrical connections and *I–V* curves show that the fabricated holders can be used for normal probe characterization, while their application in SICM and P-SICM to obtain topography maps and simultaneously collected, correlative topography and local apparent conductance maps, respectively, demonstrate that these holders can be used in more rigorous experiments. Although, the cost-effective advantage of producing homebuilt holders is beneficial, a more significant advantage is the ability to customize design to experimental need. An example of this, seen in Fig. 6, that goes beyond production of a simple single or theta barrel electrode holder, builds more complex holder designs that have additional side ports for pressure connections (Fig. 6a) or the addition of a threaded port for an auxiliary electrical connection (Fig. 6b).

Finally, consideration of the end application of 3D SLA printing by means of rapid prototyping devices should be made, as demonstrated in the case of SPM experiments where physical properties of the resin dictated quality of experimental results obtained. Solutions to problems, such as those addressed in

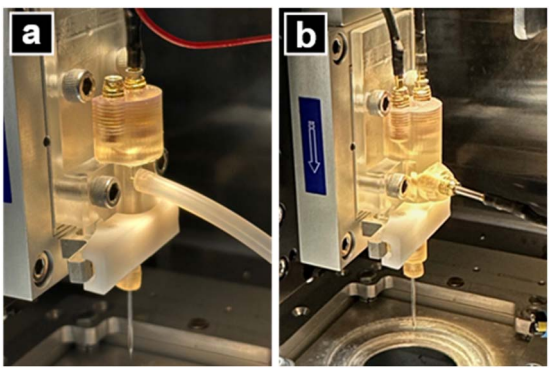

Fig. 6 Customization of electrode holders. (a) Image of an electrode holder for theta barrel probes that has two electrical connections at the top and a side port that allows for tube connections for electrophysiological experiments. (b) Image of an electrode holder for multibarrel probes that has two electrical connections at the top and a third along the holder's body orthogonal to the body of the holder.

this work, shows that some 3D printers and their respective resins may not be best suited for fabricating pivotal parts of SPM experiments. As printing technology advances, further exploration of the production quality more economical printers/resins that offer different material properties is an important avenue to consider. This could include printing the holders in glass.

Data availability

The data supporting this article have been included in ESI.†

Conflicts of interest

There are no conflicts to declare.

Acknowledgements

Electron microscopy was conducted in Texas A&M University Materials Characterization Core Facility (RRID:SCR_022202), which is supported by the Division of Research, the College of Engineering/TEES, and the College of Arts & Sciences, Texas A&M University. Formlabs printing was conducted in Texas A&M University Fischer Engineering Design Center Prototyping Center. This work was funded by the U.S. Army Research Office (W911NF2210051) to LAB.

References

1 W. Bai, H. Fang, Y. Wang, Q. Zeng, G. Hu, G. Bao and Y. Wan, *Appl. Sci.*, 2021, **11**, 8298.
2 S. Volpe, V. Sangiorgio, F. Fiorito and H. Varum, *Archit. Sci. Rev.*, 2024, **67**, 1–22.
3 F. L. Buchauer, A. Russo, E. R. Moretti, S. Iqbal, M. R. Kraglund and C. Chatzichristodoulou, *Electrochim. Acta*, 2024, **500**, 144719.
4 R. D. Crapnell and C. E. Banks, *Anal. Methods*, 2024, **16**, 2625–2634.
5 F. M. de Oliveira, M. Z. Martins Mendonca, N. C. de Moraes, J. M. Petroni, M. M. Neves, E. I. de Melo, B. G. Lucca and R. A. Bezerra da Silva, *Anal. Methods*, 2022, **14**, 3345–3354.
6 V. W. dos Santos, G. Martins, J. L. Gogola, C. Kalinke, D. Agustini, M. F. Bergamini and L. H. Marcolino-Junior, *Anal. Methods*, 2023, **15**, 4862–4869.
7 M. Deka, N. Sinha, R. Das, N. K. Hazarika, H. Das, B. Daurai and M. Gogoi, *Anal. Methods*, 2024, **16**, 485–495.
8 H. Agrawaal and J. E. Thompson, *Talanta Open*, 2021, **3**, 100036.
9 M. J. Whittingham, R. D. Crapnell, E. J. Rothwell, N. J. Hurst and C. E. Banks, *Talanta Open*, 2021, **4**, 100051.
10 M. J. Whittingham, R. D. Crapnell and C. E. Banks, *Anal. Chem.*, 2022, **94**, 13540–13548.
11 G. M. da Penha, A. V. Pereira, E. A. Tavares, D. A. dos Santos Jr and O. Fatibello-Filho, *Anal. Methods*, 2024, **16**, 5676–5683.
12 A. Kathiravan, S. Sengottiyan, T. Puzyn, P. Gopinath, K. Ramasubramanian, P. A. Susila and M. A. Jhonsi, *Anal. Methods*, 2022, **14**, 518–525.
13 F. Pettinau, B. Pittau and A. Orru, *Anal. Methods*, 2023, **15**, 2935–2945.
14 E. A. Hayter, S. Azibere, L. A. Skrajewski, L. D. Soule, D. M. Spence and R. S. Martin, *Anal. Methods*, 2022, **14**, 3171–3179.
15 T. Hu, W. Han, Y. Zhou, W. Tu, X. Li and Z. Ni, *Anal. Methods*, 2024, **16**, 5335–5344.
16 K. Cenhrang, L. Robart, A. D. Castiaux and R. S. Martin, *Anal. Chim. Acta*, 2022, **1221**, 340166.
17 M. A. Selemani, K. Cenhrang, S. Azibere, M. Singhateh and R. S. Martin, *Anal. Methods*, 2024, **16**, 6941–6953.
18 A. D. Castiaux, C. W. Pinger, E. A. Hayter, M. E. Bunn, R. S. Martin and D. M. Spence, *Anal. Chem.*, 2019, **91**, 6910–6917.
19 A. D. Castiaux, M. A. Selemani, M. A. Ward and R. S. Martin, *Anal. Methods*, 2021, **13**, 5017–5024.
20 E. R. Currens, M. R. Armbruster, A. D. Castiaux, J. L. Edwards and R. S. Martin, *Anal. Bioanal. Chem.*, 2022, **414**, 3329–3339.
21 K. B. Anderson, S. Y. Lockwood, R. S. Martin and D. M. Spence, *Anal. Chem.*, 2013, **85**, 5622–5626.
22 C. Chen, B. T. Mehl, A. S. Munshi, A. D. Townsend, D. M. Spence and R. S. Martin, *Anal. Methods*, 2016, **8**, 6005–6012.
23 J. L. Erkal, A. Selimovic, B. C. Gross, S. Y. Lockwood, E. L. Walton, S. McNamara, R. S. Martin and D. M. Spence, *Lab Chip*, 2014, **14**, 2023–2032.
24 B. Gross, S. Y. Lockwood and D. M. Spence, *Anal. Chem.*, 2017, **89**, 57–70.
25 D. R. Eitzmann and J. L. Anderson, *Anal. Methods*, 2022, **14**, 2682–2688.
26 K. Teng, J. Shi, Y. Zhu and Q. Yu, *Anal. Methods*, 2022, **14**, 4886–4892.
27 I. Hietanen, I. T. S. Heikkinen, H. Savin and J. M. Pearce, *HardwareX*, 2018, **4**, e00042.
28 G. N. Meloni, *Anal. Chem.*, 2017, **89**, 8643–8649.
29 C.-C. Chen and L. A. Baker, *Analyst*, 2011, **136**, 90–97.
30 K. Alanis, Z. S. Siwy and L. A. Baker, *J. Electrochem. Soc.*, 2023, **170**, 066510.
31 K. Huang, L. Zhou, K. Alanis, J. Hou and L. A. Baker, *Chem. Sci.*, 2020, **11**, 1307–1315.
32 Y. Zhou, L. K. Bright, W. Shi, C. A. Aspinwall and L. A. Baker, *Langmuir*, 2014, **30**, 15351–15355.
33 C. Zhu, K. Huang, Y. Wang, K. Alanis, W. Shi and L. A. Baker, *Anal. Chem.*, 2021, **93**, 5355–5359.
34 K. Shigyou, L. Sun, R. Yajima, S. Takigaura, M. Tajima, H. Furusho, Y. Kikuchi, K. Miyazawa, T. Fukuma, A. Taoka, T. Ando and S. Watanabe, *Anal. Chem.*, 2020, **92**, 15388–15393.
35 M. Choi and L. A. Baker, *Anal. Chem.*, 2018, **90**, 11797–11801.
36 J. Kim, M. Shen, N. Nioradze and S. Amemiya, *Anal. Chem.*, 2012, **84**, 3489–3492.
37 C.-C. Chen, Y. Zhou, C. A. Morris, J. Hou and L. A. Baker, *Anal. Chem.*, 2013, **85**, 3621–3628.
38 Y. Zhou, C.-C. Chen, A. E. Weber, L. Zhou and L. A. Baker, *Langmuir*, 2014, **30**, 5669–5675.
39 M. Lavallée, N. C. Hébert and O. F. Schanne, *Glass Microelectrodes*, Wiley, New York, London, 1969.

40 K. Alanis, S. E. Alden, L. A. Baker, E. S. Anupriya, H. D. Jetmore and M. Shen, in *Scanning Electrochemical Microscopy*, CRC Press, Boca Raton, 3rd edn, 2022, pp. 419–480.
41 N. P. Siepser, PhD dissertation, Indiana University, 2022.
42 M. Choi, N. P. Siepser, S. Jeong, Y. Wang, G. Jagdale, X. Ye and L. A. Baker, *Nano Lett.*, 2020, **20**, 1233–1239.
43 L. Zhou, Y. Gong, J. Hou and L. A. Baker, *Anal. Chem.*, 2017, **89**, 13603–13609.